Blast Response of a Sandwich Beam/Wide Plate Based on the Extended High-Order Sandwich Panel Theory and Comparison With Elasticity

Catherine N. Phan[1]
Graduate Research Assistant

George A. Kardomateas
Professor

Yeoshua Frostig[2]

School of Aerospace Engineering,
Georgia Institute of Technology,
Atlanta, GA 30332-0150

This paper presents a one-dimensional analysis for the blast response of a sandwich beam/wide plate with a compressible core. The dynamic version of the recently developed extended high-order sandwich panel theory (EHSAPT) is first formulated. Material, geometric, and loading parameters are taken from blast experiments reported in literature. The novelty of EHSAPT is that it includes axial rigidity of the core and allows for three generalized coordinates in the core (the axial and transverse displacements at the centroid of the core and the rotation at the centroid of the core) instead of just one (shear stress in the core) of the earlier high-order sandwich panel theory (HSAPT). The solution procedure to determine the dynamic response to a general load applied on the top face sheet of a general asymmetric simply supported configuration is outlined. Although the dynamic EHSAPT is formulated in its full nonlinear version, the solution is for the linear problem so the accuracy of EHSAPT, along with the other theories, can be assessed by comparison to an available dynamic elasticity solution. Results show that the EHSAPT is very accurate and can capture the complex dynamic phenomena observed during the initial, transient phase of blast loading. [DOI: 10.1115/1.4023619]

1 Introduction

Sandwich composites are utilized in the naval, aerospace, and wind engineering industries for their beneficial properties of high stiffness and strength while being lightweight. The sandwich configuration consists of two thin stiff face sheets and a thick low density core material as depicted in Fig. 1. Such structures may be subjected to highly transient loads such as blast, gusts, or impact, with surface pressure spread over the entire structure or over a certain area. It is believed that if the structure survives the initial, transient phase of blast loading (time scale of a few milliseconds) then it has survived the blast. Thus, the transient response of suddenly loaded structural configurations is essential in ensuring their integrity. In the study of the response of a sandwich structure subject to static loading or a dynamic loading of long duration, it has been customary to neglect the deformation of the core in the transverse direction as shown in the early textbooks of Allen (1969) [1] and Plantema (1966) [2]. Under this simplifying assumption, the core is assumed to be infinitely rigid in the thickness direction and can only carry the shear stresses. This model has been shown to be inaccurate in predicting displacements for very soft core sandwich configurations under quasi-static loading (Kardomateas and Phan [3]). More importantly, experimental results [4–8] have shown that the core can undergo significant transverse deformation when the sandwich structure experiences a sudden, impulsive loading and the core plays an important role in the absorption of the impact energy. Therefore, a more accurate sandwich composite model should account for the transverse compressibility of the core.

In 1992, Frostig et al. [9] developed the high-order sandwich panel theory (HSAPT), a compressible core theory that accounts for the transverse and shear rigidity of the core but neglects the axial rigidity of the core. Neglecting the axial rigidity of the core results in a constant shear stress distribution through the thickness of the core that is a good approximation for sandwich constructions with very soft cores undergoing quasi-static loading [3]. Recently, the extended high-order sandwich panel theory (EHSAPT) has been formulated to account for the axial, transverse, and shear rigidity of the core (Phan et al. [10]). This new theory includes the axial rigidity of the core and allows for an accurate prediction of the shear stress distribution through the thickness of the core in a wide range of core stiffnesses [10].

In the authors' previous work (Phan et al. [10]) the EHSAPT was presented in its static version and the accuracy of all the high-order theories was assessed for static problems. In this paper we shall assess the theories for a dynamical loading problem. In this paper the dynamic version (equations of motion and boundary conditions) of the new EHSAPT is presented. A solution

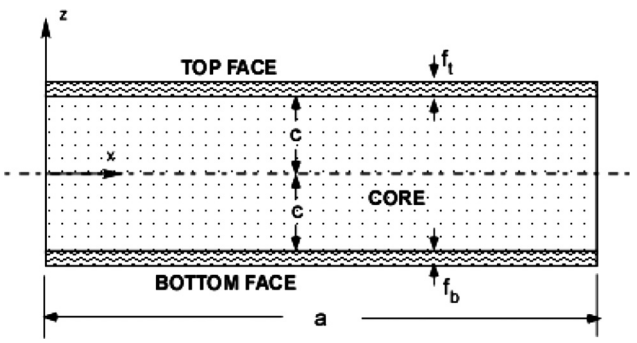

Fig. 1 Definition of the sandwich configuration

[1]Presently an Engineer/Scientist at Dynamic Concepts, Inc., Huntsville, AL.
[2]Professor of Structural Engineering, Technion Israel Institute of Technology, Haifa 32 000, Israel.

Manuscript received June 20, 2012; final manuscript received December 20, 2012; accepted manuscript posted February 11, 2013; published online August 19, 2013. Assoc. Editor: Weinong Chen.

procedure to obtain the response of a simply supported sandwich beam to a dynamic load applied on the top face is outlined. The sandwich composite is of a general asymmetric construction, and the dynamic load has a general spatial and temporal profile. The solution is for the linear response so comparison can be made with an elastodynamic solution of the same problem, which was recently formulated (Kardomateas et al. [11]).

A numerical case study was chosen using the material, geometry, and blast loading data that were reported in the blast experiments of Gardner et al. [4]. The load is simplified to half-sine distributed load that exponentially decays in time. Comparison between EHSAPT, HSAPT, and elasticity is made for displacements and stresses. Additional results for the shear stresses are shown for EHSAPT and HSAPT for two other sandwich configurations: one that represents a sandwich composite with a very soft core and another that represents a sandwich composite with a moderate core, both with very thin faces. The paper ends with conclusions.

2 Formulation of the Governing Equations of Motion

Figure 1 shows a sandwich panel of length a with a core of thickness $2c$ and top and bottom face sheet thicknesses f_t and f_b, respectively. A unit width of the beam is assumed. A Cartesian coordinate system (x, y, z) is defined at one end of the beam and its origin is placed at the middle of the core. Only loading in the $x-z$ plane is considered to act on the beam that solely causes displacements in the x and z directions designated by u and w, respectively. The superscripts t, b, and c shall refer to the top face sheet, bottom face sheet, and core, respectively. The subscript 0 refers to the middle surface of the corresponding phase.

The displacement field of the top and bottom face sheets is assumed to satisfy the Euler–Bernoulli assumptions: that planes remain plane and perpendicular to the constituent's deformed axis, and the face sheets are infinitely rigid in the transverse direction. Therefore, the displacement field for the top face sheet $c \le z \le c + f_t$ is

$$w^t(x,z,t) = w_0^t(x,t);$$
$$u^t(x,z,t) = u_0^t(x,t) - \left(z - c - \frac{f_t}{2}\right) w_{0,x}^t,(x,t) \tag{1a}$$

and for the bottom face sheet $-(c+f_b) \le z \le -c$

$$w^b(x,z,t) = w_0^b(x,t);$$
$$u^b(x,z,t) = u_0^b(x,t) - \left(z + c + \frac{f_b}{2}\right) w_{0,x}^b,(x,t) \tag{1b}$$

The only nonzero strain in the faces is the axial strain, which in the general nonlinear case (necessary, for example, for buckling) is

$$\epsilon_{x,x}^{t,b}(x,z,t) = u_x^{t,b}(x,z,t) + \frac{1}{2}\left[w_{0,x}^{t,b}(x,t)\right]^2 \tag{1c}$$

If a linear analysis is pursued, the second (squared) term in Eq. (1c) is neglected.

While the face sheets can change their length only longitudinally, the core can change its height and length. The displacement field that satisfies the compatibility conditions at the upper and the lower face core interfaces (same core and face sheet transverse and axial displacements) is (Phan et al. [10])

$$w^c(x,z,t) = \left(-\frac{z}{2c} + \frac{z^2}{2c^2}\right) w_0^b(x,t) + \left(1 - \frac{z^2}{c^2}\right) w_0^c(x,t) + \left(\frac{z}{2c} + \frac{z^2}{2c^2}\right) w_0^t(x,t) \tag{2a}$$

$$u^c(x,z,t) = z\left(1 - \frac{z^2}{c^2}\right)\phi_0^c(x,t) + \frac{z^2}{2c^2}\left(1 - \frac{z}{c}\right)u_0^b + \left(1 - \frac{z^2}{c^2}\right)u_0^c + \frac{z^2}{2c^2}\left(1 + \frac{z}{c}\right)u_0^t + \frac{f_b z^2}{4c^2}\left(-1 + \frac{z}{c}\right)w_{0,x}^b + \frac{f_t z^2}{4c^2}\left(1 + \frac{z}{c}\right)w_{0,x}^t \tag{2b}$$

where w_0^c and u_0^c are the transverse and in-plane displacements, respectively, and ϕ_0^c is the slope at the centroid of the core.

Therefore, this theory is in terms of seven generalized coordinates (unknown functions of x and t): two for the top face sheet, w_0^t, u_0^t; two for the bottom face sheet, w_0^b, u_0^b; and three for the core, w_0^c, u_0^c, and ϕ_0^c.

The strains can be obtained from the displacements using the linear strain-displacement relations. The explicit relationships for the transverse normal and the shear strain in the core can also be found in Phan et al. [10]. There is also a nonzero linear axial strain in the core ϵ_{xx}^c, which has the same structure as Eq. (2b) but with the generalized function coordinates replaced by one order higher derivative with respect to x.

In the following $C_{ij}^{t,b,c}$ are the corresponding stiffness constants and we have used the notation $1 \equiv x$, $3 \equiv z$, and $55 \equiv xz$. We assume orthotropic face sheets; thus, the nonzero stresses for the faces are

$$\sigma_{xx}^{t,b} = C_{11}^{t,b}\epsilon_{xx}^{t,b}; \quad \sigma_{zz}^{t,b} = C_{13}^{t,b}\epsilon_{xx}^{t,b} \tag{3a}$$

where, in terms of the extensional (Young's) modulus $E_1^{t,b}$ and the Poisson's ratio $\nu_{31}^{t,b}$, the stiffness constants for a beam are $C_{11}^{t,b} = E_1^{t,b}$ and $C_{13}^{t,b} = \nu_{31}^{t,b}E_1^{t,b}$. Notice that the $\sigma_{zz}^{t,b}$ does not ultimately enter into the variational equation because the corresponding strain $\epsilon_{zz}^{t,b}$ is zero.

We also assume an orthotropic core with stress-strain relations

$$\begin{bmatrix} \sigma_{xx}^c \\ \sigma_{zz}^c \\ \tau_{xz}^c \end{bmatrix} = \begin{bmatrix} C_{11}^c & C_{13}^c & 0 \\ C_{13}^0 & C_{33}^c & 0 \\ 0 & 0 & C_{55}^c \end{bmatrix} \begin{bmatrix} \epsilon_{xx}^c \\ \epsilon_{zz}^c \\ \gamma_{xz}^c \end{bmatrix} \tag{3b}$$

where the components C_{ij}^c constitute the stiffness matrix, which is the inverse of the compliance matrix, whose components a_{ij}^c are expressed in terms of the extensional and shear moduli and Poisson's ratio of the core as

$$a_{11}^c = \frac{1}{E_1^c}; \quad a_{13}^c = -\frac{\nu_{31}^c}{E_3^c}; \quad a_{33}^c = \frac{1}{E_3^c}; \quad a_{55}^c = \frac{1}{G_{31}^c} \tag{3c}$$

The equations of motion and appropriate boundary conditions are derived from Hamilton's principle

$$\int_{t_1}^{t_2} \delta(U + V - T)dt = 0 \tag{4a}$$

where U is the strain energy of the sandwich beam, V is the potential due to the applied loading, and T is the kinetic energy. The first variation of the strain energy of the sandwich beam and the first variation of the external potential due to several general loading conditions can be found in Phan et al. [10].

The kinetic energy term is

$$\delta T = \int_0^a \int_0^b \left[\int_{-(c+f_b)}^{-c} \rho^b(\dot{u}^b\delta\dot{u}^b + \dot{w}^b\delta\dot{w}^b)dz + \int_{-c}^{c} \rho^c(\dot{u}^c\delta\dot{u}^c + \dot{w}^c\delta\dot{w}^c)dz + \int_{c}^{c+f_t} \rho^t(\dot{u}^t\delta\dot{u}^t + \dot{w}^t\delta\dot{w}^t)dz \right] dydx \tag{4b}$$

where ρ is the mass density. The superscript t denotes the corresponding quantity for the top face sheet, whereas t, when appearing in the variables list of a function, refers to time.

For the sandwich plates made out of orthotropic materials, we can substitute the stresses in terms of the strains from the constitutive relations and then the strains in terms of the displacements and the displacement profiles and finally apply the variational principle; thus, we can write a set of nonlinear governing equations in terms of the seven unknown generalized coordinates as follows.

Top Face Sheet

$$\begin{aligned}\delta u_0^t :& -\left(\frac{4}{5}C_{55}^c+\frac{2c^2}{35}C_{11}^c\frac{\partial^2}{\partial x^2}-\frac{2c^2\rho^c}{35}\frac{\partial^2}{\partial t^2}\right)\phi_0^c\\ &-\left(\frac{7}{30c}C_{55}^c+\frac{c}{35}C_{11}^c\frac{\partial^2}{\partial x^2}-\frac{c\rho^c}{35}\frac{\partial^2}{\partial t^2}\right)u_0^b\\ &-\left(\frac{4}{3c}C_{55}^c+\frac{2c}{15}C_{11}^c\frac{\partial^2}{\partial x^2}-\frac{2c\rho^c}{15}\frac{\partial^2}{\partial t^2}\right)u_0^c\\ &+\left[\frac{47}{30c}C_{55}^c-\alpha_1^t\frac{\partial^2}{\partial x^2}+\left(\frac{6c\rho^c}{35}+f_t\rho^t\right)\frac{\partial^2}{\partial t^2}\right]u_0^t\\ &-\left(\alpha_2^b\frac{\partial}{\partial x}-\frac{cf_b}{70}C_{11}^c\frac{\partial^3}{\partial x^3}+\frac{cf_b\rho^c}{70}\frac{\partial^3}{\partial x\partial t^2}\right)w_0^b+\left(\beta_1\frac{\partial}{\partial x}\right)w_0^c\\ &+\left(\alpha_3^t\frac{\partial}{\partial x}-\frac{3cf_t}{35}C_{11}^c\frac{\partial^3}{\partial x^3}+\frac{3cf_t\rho^c}{35}\frac{\partial^3}{\partial x\partial t^2}\right)w_0^t=\tilde{p}^t+F_u^t\end{aligned}\tag{5a}$$

where F_u^t is the nonlinear term

$$F_u^t=C_{11}^t f_t w_{0,x}^t w_{0,xx}^t\tag{5b}$$

and $\tilde{p}^t$ is the distributed in-plane force (along x) per unit width at the top face, and

$$\begin{aligned}\delta w_0^t :&\left(\alpha_4^t\frac{\partial}{\partial x}+\frac{c^2f_t}{35}C_{11}^c\frac{\partial^3}{\partial x^3}-\frac{c^2f_t\rho^c}{35}\frac{\partial^3}{\partial x\partial t^2}\right)\phi_0^c\\ &+\left(\alpha_5^t\frac{\partial}{\partial x}+\frac{cf_t}{70}C_{11}^c\frac{\partial^3}{\partial x^3}-\frac{cf_t\rho^c}{70}\frac{\partial^3}{\partial x\partial t^2}\right)u_0^b\\ &+\left(\alpha_6^t\frac{\partial}{\partial x}+\frac{cf_t}{15}C_{11}^c\frac{\partial^3}{\partial x^3}-\frac{cf_t\rho^c}{15}\frac{\partial^3}{\partial x\partial t^2}\right)u_0^c\\ &+\left(-\alpha_3^t\frac{\partial}{\partial x}+\frac{3cf_t}{35}C_{11}^c\frac{\partial^3}{\partial x^3}-\frac{3cf_t\rho^c}{35}\frac{\partial^3}{\partial x\partial t^2}\right)u_0^t\\ &+\left(\frac{1}{6c}C_{33}^c+\beta_2\frac{\partial^2}{\partial x^2}-\frac{cf_bf_t}{140}C_{11}^c\frac{\partial^4}{\partial x^4}-\frac{c\rho^c}{15}\frac{\partial^2}{\partial t^2}\right.\\ &\left.+\frac{cf_bf_t\rho^c}{140}\frac{\partial^4}{\partial x^2\partial t^2}\right)w_0^b+\left(-\frac{4}{3c}C_{33}^c+\alpha_7^t\frac{\partial^2}{\partial x^2}+\frac{2c\rho^c}{15}\frac{\partial^2}{\partial t^2}\right)w_0^c\\ &+\left[\frac{7}{6c}C_{33}^c+\alpha_8^t\frac{\partial^2}{\partial x^2}+\alpha_9^t\frac{\partial^4}{\partial x^4}+\left(\frac{4c\rho^c}{15}+f_t\rho^t\right)\frac{\partial^2}{\partial t^2}\right.\\ &\left.-\left(\frac{3cf_t^2\rho^c}{70}+\frac{f_t^3\rho^t}{12}\right)\frac{\partial^4}{\partial x^2\partial t^2}\right]w_0^t=\tilde{q}^t-\tilde{m}_{,x}^t+F_w^t\end{aligned}\tag{6a}$$

where F_w^t is the nonlinear term

$$F_w^t=C_{11}^t f_t\left[w_{0,x}^t u_{0,xx}^t+u_{0,x}^t w_{0,xx}^t+\frac{3}{2}(w_{0,x}^t)^2 w_{0,xx}^t\right]\tag{6b}$$

and $\tilde{q}^t$ is the distributed transverse force (along z) per unit width and $\tilde{m}^t$ is the distributed moment per unit width along the top face sheet.

Core

$$\begin{aligned}\delta u_0^c :& -\left(\frac{4}{3c}C_{55}^c+\frac{2c}{15}C_{11}^c\frac{\partial^2}{\partial x^2}-\frac{2c\rho^c}{15}\frac{\partial^2}{\partial t^2}\right)u_0^b\\ &+\left(\frac{8}{3c}C_{55}^c-\frac{16c}{15}C_{11}^c\frac{\partial^2}{\partial x^2}+\frac{16c\rho^c}{15}\frac{\partial^2}{\partial t^2}\right)u_0^c\\ &-\left(\frac{4}{3c}C_{55}^c+\frac{2c}{15}C_{11}^c\frac{\partial^2}{\partial x^2}-\frac{2c\rho^c}{15}\frac{\partial^2}{\partial t^2}\right)u_0^t\\ &+\left(\alpha_6^b\frac{\partial}{\partial x}+\frac{cf_b}{15}C_{11}^c\frac{\partial^3}{\partial x^3}-\frac{cf_b\rho^c}{15}\frac{\partial^3}{\partial x\partial t^2}\right)w_0^b\\ &-\left(\alpha_6^t\frac{\partial}{\partial x}+\frac{cf_t}{15}C_{11}^c\frac{\partial^3}{\partial x^3}-\frac{cf_t\rho^c}{15}\frac{\partial^3}{\partial x\partial t^2}\right)w_0^t=0\end{aligned}\tag{7}$$

$$\begin{aligned}\delta\phi_0^c :&\left(\frac{8c}{5}C_{55}^c-\frac{16c^3}{105}C_{11}^c\frac{\partial^2}{\partial x^2}+\frac{16c^3\rho^c}{105}\frac{\partial^2}{\partial t^2}\right)\phi_0^c\\ &+\left(\frac{4}{5}C_{55}^c+\frac{2c^2}{35}C_{11}^c\frac{\partial^2}{\partial x^2}-\frac{2c^2\rho^c}{35}\frac{\partial^2}{\partial t^2}\right)u_0^b\\ &-\left(\frac{4}{5}C_{55}^c+\frac{2c^2}{35}C_{11}^c\frac{\partial^2}{\partial x^2}-\frac{2c^2\rho^c}{35}\frac{\partial^2}{\partial t^2}\right)u_0^t\\ &-\left(\alpha_4^b\frac{\partial}{\partial x}+\frac{c^2f_b}{35}C_{11}^c\frac{\partial^3}{\partial x^3}-\frac{c^2f_b\rho^c}{35}\frac{\partial^3}{\partial x\partial t^2}\right)w_0^b+\left(\beta_3\frac{\partial}{\partial x}\right)w_0^c\\ &-\left(\alpha_4^t\frac{\partial}{\partial x}+\frac{c^2f_t}{35}C_{11}^c\frac{\partial^3}{\partial x^3}-\frac{c^2f_t\rho^c}{35}\frac{\partial^3}{\partial x\partial t^2}\right)w_0^t=0\end{aligned}\tag{8}$$

and

$$\begin{aligned}\delta w_0^c :& -\left(\beta_3\frac{\partial}{\partial x}\right)\phi_0^c+\left(\beta_1\frac{\partial}{\partial x}\right)u_0^b-\left(\beta_1\frac{\partial}{\partial x}\right)u_0^t\\ &+\left(-\frac{4}{3c}C_{33}^c+\alpha_7^b\frac{\partial^2}{\partial x^2}+\frac{2c\rho^c}{15}\frac{\partial^2}{\partial t^2}\right)w_0^b\\ &+\left(\frac{8}{3c}C_{33}^c-\frac{16c}{15}C_{55}^c\frac{\partial^2}{\partial x^2}+\frac{16c\rho^c}{15}\frac{\partial^2}{\partial t^2}\right)w_0^c\\ &+\left(-\frac{4}{3c}C_{33}^c+\alpha_7^t\frac{\partial^2}{\partial x^2}+\frac{2c\rho^c}{15}\frac{\partial^2}{\partial t^2}\right)w_0^t=0\end{aligned}\tag{9}$$

Bottom Face Sheet

$$\begin{aligned}\delta u_0^b :&\left(\frac{4}{5}C_{55}^c+\frac{2c^2}{35}C_{11}^c\frac{\partial^2}{\partial x^2}-\frac{2c^2\rho^c}{35}\frac{\partial^2}{\partial t^2}\right)\phi_0^c\\ &+\left(\frac{47}{30c}C_{55}^c-\alpha_1^b\frac{\partial^2}{\partial x^2}+\left(\frac{6c\rho^c}{35}+f_b\rho^b\right)\frac{\partial^2}{\partial t^2}\right)u_0^b\\ &-\left(\frac{4}{3c}C_{55}^c+\frac{2c}{15}C_{11}^c\frac{\partial^2}{\partial x^2}-\frac{2c\rho^c}{15}\frac{\partial^2}{\partial t^2}\right)u_0^c\\ &-\left(\frac{7}{30c}C_{55}^c+\frac{c}{35}C_{11}^c\frac{\partial^2}{\partial x^2}-\frac{c\rho^c}{35}\frac{\partial^2}{\partial t^2}\right)u_0^t\\ &+\left(-\alpha_3^b\frac{\partial}{\partial x}+\frac{3cf_b}{35}C_{11}^c\frac{\partial^3}{\partial x^3}-\frac{3cf_b\rho^c}{35}\frac{\partial^3}{\partial x\partial t^2}\right)w_0^b-\left(\beta_1\frac{\partial}{\partial x}\right)w_0^c\\ &+\left(\alpha_2^t\frac{\partial}{\partial x}-\frac{cf_t}{70}C_{11}^c\frac{\partial^3}{\partial x^3}+\frac{cf_t\rho^c}{70}\frac{\partial^3}{\partial x\partial t^2}\right)w_0^t=\tilde{p}^b+\hat{F}_u^b\end{aligned}\tag{10a}$$

where F_u^b is the nonlinear term

$$F_u^b=C_{11}^b bf_b w_{0,x}^b w_{0,xx}^b\tag{10b}$$

and $\tilde{p}^b$ is the distributed in-plane force (along x) per unit width at the bottom face, and

$$\delta w_0^b : \left(\alpha_4^b \frac{\partial}{\partial x} + \frac{c^2 f_b}{35} C_{11}^c \frac{\partial^3}{\partial x^3} - \frac{c^2 f_b \rho^c}{35} \frac{\partial^3}{\partial x \partial t^2}\right) \phi_0^c + \left(\alpha_3^b \frac{\partial}{\partial x} - \frac{3cf_b}{35} C_{11}^c \frac{\partial^3}{\partial x^3} + \frac{3cf_b \rho^c}{35} \frac{\partial^3}{\partial x \partial t^2}\right) u_0^b - \left(\alpha_6^b \frac{\partial}{\partial x} + \frac{cf_b}{15} C_{11}^c \frac{\partial^3}{\partial x^3} - \frac{cf_b \rho^c}{15} \frac{\partial^3}{\partial x \partial t^2}\right) u_0^c - \left(\alpha_5^b \frac{\partial}{\partial x} + \frac{cf_b}{70} C_{11}^c \frac{\partial^3}{\partial x^3} - \frac{cf_b \rho^c}{70} \frac{\partial^3}{\partial x \partial t^2}\right) u_0^t + \left(\frac{7}{6c} C_{33}^c + \alpha_8^b \frac{\partial^2}{\partial x^2} + \alpha_9^b \frac{\partial^4}{\partial x^4} + \left(\frac{4c\rho^c}{15} + f_b \rho^b\right) \frac{\partial^2}{\partial t^2} - \left(\frac{3cf_b^2 \rho^c}{70} + \frac{f_b^3 \rho^b}{12}\right) \frac{\partial^4}{\partial x^2 \partial t^2}\right) w_0^b + \left(-\frac{4}{3c} C_{33}^c + \alpha_7^b \frac{\partial^2}{\partial x^2} + \frac{2c\rho^c}{15} \frac{\partial^2}{\partial t^2}\right) w_0^c + \left(\frac{1}{6c} C_{33}^c + \beta_2 \frac{\partial^2}{\partial x^2} - \frac{cf_b f_t}{140} C_{11}^c \frac{\partial^4}{\partial x^4} - \frac{c\rho^c}{15} \frac{\partial^2}{\partial t^2} + \frac{cf_b f_t \rho^c}{140} \frac{\partial^4}{\partial x^2 \partial t^2}\right) w_0^t = \tilde{q}^b - \tilde{m}_{,x}^b + F_w^b \tag{11a}$$

where F_w^b is the nonlinear term

$$F_w^b = C_{11}^b b f_b \left[w_{0,x}^b u_{0,xx}^b + u_{0,x}^b w_{o,xx}^b + \frac{3}{2}(w_{0,x}^b)^2 w_{0,xx}^b\right] \tag{11b}$$

and $\tilde{q}^b$ is the distributed transverse force per unit width and $\tilde{m}^b$ is the distributed moment applied per unit width along the bottom face sheet.

In the above expressions, the following constants are defined:

$$\alpha_1^i = \frac{6c}{35} C_{11}^c + f_i C_{11}^i; \quad \alpha_2^i = \frac{1}{30} C_{13}^c + \left(\frac{1}{30} - \frac{7f_i}{60c}\right) C_{55}^c \tag{12a}$$

$$\alpha_3^i = -\frac{11}{30} C_{13}^c + \left(\frac{19}{30} + \frac{47f_i}{60c}\right) C_{55}^c; \quad \alpha_4^i = \frac{4c}{15} C_{13}^c + \left(\frac{4c}{15} + \frac{2f_i}{5}\right) C_{55}^c \tag{12b}$$

$$\alpha_5^i = -\alpha_2^i; \quad \alpha_6^i = \frac{2}{3} C_{13}^c + \left(\frac{2}{3} + \frac{2f_i}{3c}\right) C_{55}^c \tag{12c}$$

$$\alpha_7^i = -\frac{f_i}{5} C_{13}^c - \left(\frac{2c}{15} + \frac{f_i}{5}\right) C_{55}^c \tag{12d}$$

$$\alpha_8^i = \frac{11f_i}{30} C_{13}^c - \left(\frac{4c}{15} + \frac{19f_i}{30} + \frac{47f_i^2}{120c}\right) C_{55}^c \tag{12e}$$

$$\alpha_9^i = \frac{f_i^3}{12} C_{11}^i + \frac{3cf_i^2}{70} C_{11}^c \tag{12f}$$

and

$$\beta_1 = \frac{2}{5}(C_{13}^c + C_{55}^c) \tag{13a}$$

$$\beta_2 = \frac{f_b + f_t}{60} C_{13}^c + \left(\frac{c}{15} + \frac{f_b + f_t}{60} - \frac{7f_b f_t}{120c}\right) C_{55}^c \tag{13b}$$

The corresponding boundary conditions at $x = 0$ and a read as follows (at each end there are nine boundary conditions, three for each of the two face sheets and three for the core).

For the top face sheet:

(i) Either $\delta u_0^t = 0$, or

$$\left(\frac{2c^2}{35} C_{11}^c \frac{\partial}{\partial x}\right) \phi_0^c + \left(\frac{c}{35} C_{11}^c \frac{\partial}{\partial x}\right) u_0^b + \left(\frac{2c}{15} C_{11}^c \frac{\partial}{\partial x}\right) u_0^c + \left(\alpha_1^t \frac{\partial}{\partial x}\right) u_0^t + \left(\frac{1}{30} C_{13}^c - \frac{cf_b}{70} C_{11}^c \frac{\partial^2}{\partial x^2}\right) w_0^b - \left(\frac{2}{5} C_{13}^c\right) w_0^c + \left(\frac{11}{30} C_{13}^c + \frac{3cf_t}{35} C_{11}^c \frac{\partial^2}{\partial x^2}\right) w_0^t = \widetilde{N}^t + \frac{\widetilde{n}^c c}{3} + B_u^t \tag{14a}$$

where $\widetilde{N}^t$ is the end axial force at the top face per unit width and $\widetilde{n}^c$ is the (uniformly distributed) end axial force at the core per unit width (at the end $x = 0$ or $x = a$) and B_u^t is the nonlinear term

$$B_u^t = -\frac{f_t}{2} C_{11}^t (w_{0,x}^t)^2 \tag{14b}$$

(ii) Either $\delta w_0^t = 0$, or

$$-\left[\frac{2(2c + 3f_t)}{15} C_{55}^c + \frac{c^2 f_t}{35} C_{11}^c \frac{\partial^2}{\partial x^2}\right] \phi_0^c + \left[\frac{(2c - 7f_t)}{60c} C_{55}^c - \frac{cf_t}{70} C_{11}^c \frac{\partial^2}{\partial x^2}\right] u_0^b - \left[\frac{2(c + f_t)}{3c} C_{55}^c + \frac{cf_t}{15} C_{11}^c \frac{\partial^2}{\partial x^2}\right] u_0^c + \left[\frac{(38c + 47f_t)}{60c} C_{55}^c - \frac{3cf_t}{35} C_{11}^c \frac{\partial^2}{\partial x^2}\right] u_0^t + \left[\left(\frac{f_b}{60} C_{13}^c - \beta_2\right) \frac{\partial}{\partial x} + \frac{cf_b f_t}{140} C_{11}^c \frac{\partial^3}{\partial x^3}\right] w_0^b - \left(\alpha_7^t \frac{\partial}{\partial x}\right) w_0^c + \left[\left(\frac{11f_t}{60} C_{13}^c - \alpha_8^t\right) \frac{\partial}{\partial x} - \alpha_9^t \frac{\partial^3}{\partial x^3}\right] w_0^t + L_w^t = \widetilde{V}^t + \widetilde{m}^t + \frac{\widetilde{v}^c c}{3} + B_w^t \tag{15a}$$

where L_w^t is the inertial term

$$L_w^t = \frac{f_t}{420}\left[35 f_t^2 \rho^t \frac{\partial^3 w_0^t}{\partial x \partial t^2} + \rho^c \left(12c^2 \frac{\partial^2 \phi_0^c}{\partial t^2} + 6c \frac{\partial^2 u_0^b}{\partial t^2} + 28c \frac{\partial^2 u_0^c}{\partial t^2} + 36c \frac{\partial^2 u_0^t}{\partial t^2} - 3cf_b \frac{\partial^3 w_0^b}{\partial x \partial t^2} + 18cf_t \frac{\partial^3 w_0^t}{\partial x \partial t^2}\right)\right] \tag{15b}$$

and B_w^t is the nonlinear term

$$B_w^t = -\frac{ft}{2} C_{11}^t w_{0,x}^t \left[2u_{0,x}^t + (w_{0,x}^t)^2\right] \tag{15c}$$

and $\widetilde{V}^t$ is the end shear force at the top face per unit width and $\widetilde{v}^c$ is the (uniformly distributed) end shear force at the core (at the end $x = 0$ or $x = a$).

(iii) Either $\delta w_{0,x}^t = 0$, or

$$\left(\frac{c^2 f_t}{35} C_{11}^c \frac{\partial}{\partial x}\right) \phi_0^c + \left(\frac{cf_t}{70} C_{11}^c \frac{\partial}{\partial x}\right) u_0^b + \left(\frac{cf_t}{15} C_{11}^c \frac{\partial}{\partial x}\right) u_0^c + \left(\frac{3cf_t}{35} C_{11}^c \frac{\partial}{\partial x}\right) u_0^t + \left(\frac{f_t}{60} C_{13}^c - \frac{cf_b f_t}{140} C_{11}^c \frac{\partial^2}{\partial x^2}\right) w_0^b - \left(\frac{f_t}{5} C_{13}^c\right) w_0^c + \left(\frac{11f_t}{60} C_{13}^c + \alpha_9^t \frac{\partial^2}{\partial x^2}\right) w_0^t = \widetilde{M}^t + \frac{\widetilde{n}^c c f_t}{6} \tag{16}$$

where $\widetilde{M}^t$ is the end moment per unit width at the top face (at the end $x = 0$ or $x = a$).

For the core:

(i) Either $\delta u_0^c = 0$, or

$$\left(\frac{2c}{15}C_{11}^c\frac{\partial}{\partial x}\right)u_0^b + \left(\frac{16c}{15}C_{11}^c\frac{\partial}{\partial x}\right)u_0^c + \left(\frac{2c}{15}C_{11}^c\frac{\partial}{\partial x}\right)u_0^t - \left(\frac{2}{3}C_{13}^c + \frac{cf_b}{15}C_{11}^c\frac{\partial^2}{\partial x^2}\right)w_0^b + \left(\frac{2}{3}C_{13}^c + \frac{cf_t}{15}C_{11}^c\frac{\partial^2}{\partial x^2}\right)w_0^t = \frac{4\widetilde{n}^c c}{3} \tag{17}$$

(ii) Either $\delta\phi_0^c = 0$, or

$$\left(\frac{16c^3}{105}C_{11}^c\frac{\partial}{\partial x}\right)\phi_0^c - \left(\frac{2c^2}{35}C_{11}^c\frac{\partial}{\partial x}\right)u_0^b + \left(\frac{2c^2}{35}C_{11}^c\frac{\partial}{\partial x}\right)u_0^t + \left(\frac{4c}{15}C_{13}^c + \frac{c^2f_b}{35}C_{11}^c\frac{\partial^2}{\partial x^2}\right)w_0^b - \left(\frac{8c}{15}C_{13}^c\right)w_0^c + \left(\frac{4c}{15}C_{13}^c + \frac{c^2f_t}{35}C_{11}^c\frac{\partial^2}{\partial x^2}\right)w_0^t = 0 \tag{18}$$

(iii) Either $\delta w_0^c = 0$, or

$$C_{55}^c\left[\frac{8c}{15}\phi_0^c - \frac{2}{5}u_0^b + \frac{2}{5}u_0^t + \frac{(2c+3f_b)}{15}w_{0,x}^b + \frac{16c}{15}w_{0,x}^c + \frac{(2c+3f_t)}{15}w_{0,x}^t\right] = \frac{4}{3}\widetilde{v}^c c \tag{19}$$

For the bottom face sheet:

(i) Either $\delta u_0^b = 0$, or

$$-\left(\frac{2c^2}{35}C_{11}^c\frac{\partial}{\partial x}\right)\phi_0^c + \left(\alpha_1^b\frac{\partial}{\partial x}\right)u_0^b + \left(\frac{2c}{15}C_{11}^c\frac{\partial}{\partial x}\right)u_0^c + \left(\frac{c}{35}C_{11}^c\frac{\partial}{\partial x}\right)u_0^t - \left(\frac{11}{30}C_{13}^c + \frac{3cf_b}{35}C_{11}^c\frac{\partial^2}{\partial x^2}\right)w_0^b + \left(\frac{2}{5}C_{13}^c\right)w_0^c + \left(-\frac{1}{30}C_{13}^c + \frac{cf_t}{70}C_{11}^c\frac{\partial^2}{\partial x^2}\right)w_0^t = \widetilde{N}^b + \frac{\widetilde{n}^c c}{3} + B_u^b \tag{20a}$$

where $\widetilde{N}^b$ is the end axial force per unit width at the bottom face and B_u^b is the nonlinear term

$$B_u^b = -\frac{f_b}{2}C_{11}^b(w_{0,x}^b)^2 \tag{20b}$$

(ii) Either $\delta w_0^b = 0$, or

$$-\left[\frac{2(2c+3f_b)}{15}C_{55}^c + \frac{c^2f_b}{35}C_{11}^c\frac{\partial^2}{\partial x^2}\right]\phi_0^c + \left[-\frac{(38c-47f_b)}{60c}C_{55}^c + \frac{3cf_b}{35}C_{11}^c\frac{\partial^2}{\partial x^2}\right]u_0^b + \left[\frac{2(c+f_b)}{3c}C_{55}^c + \frac{cf_b}{15}C_{11}^c\frac{\partial^2}{\partial x^2}\right]u_0^c + \left[\frac{(-2c+7f_b)}{60c}C_{55}^c + \frac{cf_b}{70}C_{11}^c\frac{\partial^2}{\partial x^2}\right]u_0^t + \left[\left(\frac{11f_b}{60}C_{13}^c - \alpha_8^b\right)\frac{\partial}{\partial x} - \alpha_9^b\frac{\partial^3}{\partial x^3}\right]w_0^b - \left(\alpha_7^b\frac{\partial}{\partial x}\right)w_0^c + \left[\left(\frac{f_t}{60}C_{13}^c - \beta_2\right)\frac{\partial}{\partial x} + \frac{cf_bf_t}{140}C_{11}^c\frac{\partial^3}{\partial x^3}\right]w_0^t + L_w^b = \widetilde{V}^b + \widetilde{m}^b + \frac{\widetilde{v}^c c}{3} + B_w^b \tag{21a}$$

where L_w^b is the inertial term

$$L_w^b = \frac{f_b}{420}\left[35f_b^2\rho^b\frac{\partial^3 w_0^b}{\partial x\partial t^2} + \rho^c\left(12c^2\rho^c\frac{\partial^2\phi_0^c}{\partial t^2} - 36c\frac{\partial^2 u_0^b}{\partial t^2} - 28c\frac{\partial^2 u_0^c}{\partial t^2} - 6c\frac{\partial^2 u_0^t}{\partial t^2} + 18cf_b\frac{\partial^3 w_0^b}{\partial x\partial t^2} - 3cf_t\frac{\partial^3 w_0^t}{\partial x\partial t^2}\right)\right] \tag{21b}$$

and B_w^b is the nonlinear term

$$B_w^b = -\frac{f_b}{2}C_{11}^b w_{0,x}^b\left[2u_{0,x}^b + (w_{0,x}^b)^2\right] \tag{21c}$$

and $\widetilde{V}^b$ is the end shear force per unit width at bottom face.

(iii) Either $\delta w_{0,x}^b = 0$, or

$$\left(\frac{c^2f_b}{35}C_{11}^c\frac{\partial}{\partial x}\right)\phi_0^c - \left(\frac{3cf_b}{35}C_{11}^c\frac{\partial}{\partial x}\right)u_0^b - \left(\frac{cf_b}{15}C_{11}^c\frac{\partial}{\partial x}\right)u_0^c - \left(\frac{cf_b}{70}C_{11}^c\frac{\partial}{\partial x}\right)u_0^t + \left(\frac{11f_b}{60}C_{13}^c + \alpha_9^b\frac{\partial^2}{\partial x^2}\right)w_0^b - \left(\frac{f_b}{5}C_{13}^c\right)w_0^c + \left(\frac{f_b}{60}C_{13}^c - \frac{cf_bf_t}{140}C_{11}^c\frac{\partial^2}{\partial x^2}\right)w_0^t = \widetilde{M}^b - \frac{\widetilde{n}^c cf_b}{6} \tag{22}$$

where $\widetilde{M}^b$ is the end moment per unit width at the bottom face. The superscript $\widetilde{\ }$ denotes in the above equations the known external boundary values.

Thus, Hamilton's principle results in seven coupled partial differential equations, as given in Eqs. (5)–(13), four of which are nonlinear due to the consideration of nonlinear axial strains in the face sheets. The order of the equations of motion is 18. Therefore, there are 18 boundary conditions, nine at each end at $x = 0$ and $x = a$ given by Eqs. (14)–(22). Since the rotation of the face sheets is assumed to be the derivative of the transverse displacement with respect to x, there exists inertial terms L_w^t and L_w^b in the boundary conditions in Eqs. (15*b*) and (21*b*). The seven unknowns of EHSAPT are: $u_0^t(x,t)$, $u_0^c(x,t)$, $u_0^b(x,t)$, $\phi_0^c(x,t)$, $w_0^t(x,t)$, $w_0^c(x,t)$, and $w_0^b(x,t)$.

2.1 Dynamic Load Applied to Top Face Sheet. In this section the linear response of a sandwich beam that is initially at rest, simply supported throughout its thickness at each end, and then subjected to the load on the top face sheet

$$\widetilde{q}^t(x,t) = T(t)\sum_{n=1}^{\infty}Q_n\sin(\alpha_n x); \quad \alpha_n = \frac{n\pi}{a} \tag{23}$$

is studied. The loading profile takes a general form via a Fourier series. The solution approach is outlined next. Afterwards, a numerical case study of a blast load with a half-sine profile (only $n = 1$) is investigated. The case study is used to assess the accuracy of the high-order theories, EHSAPT and HSAPT, with the elastodynamic solution used as the benchmark.

In order to enable direct comparison with the linear elastodynamic benchmark solution, we outline the solution for the linear EHSAPT. Therefore, the nonlinear terms in the equations of motion and the boundary conditions are ignored. The boundary conditions are simply supported at both ends and throughout the entire beam thickness. Therefore, the solution must satisfy at $x = 0$ and a, the three kinematic boundary conditions

$$w_0^t = w_0^b = w_0^c = 0 \tag{24}$$

and the right-hand sides of the six natural boundary conditions in Eqs. (14*a*), (16), (17), (18), (20*a*), and (22) are equal to zero.

The following displacement shape functions satisfy these boundary conditions:

$$u_0^t = \sum_{n=1}^{\infty} U_n^t(t)\cos\frac{\pi x}{a}; \quad u_0^c = \sum_{n=1}^{\infty} U_n^c(t)\cos\frac{\pi x}{a};$$
$$\phi_0^c = \sum_{n=1}^{\infty} \Phi_n^c(t)\cos\frac{\pi x}{a}; \quad u_0^b = \sum_{n=1}^{\infty} U_n^b(t)\cos\frac{\pi x}{a},$$
$$w_0^t = \sum_{n=1}^{\infty} W_n^t(t)\sin\frac{\pi x}{a}; \quad w_0^c = \sum_{n=1}^{\infty} W_n^c(t)\sin\frac{\pi x}{a};$$
$$w_0^b = \sum_{n=1}^{\infty} W_n^b(t)\sin\frac{\pi x}{a} \tag{25}$$

Substituting Eq. (25) into Eqs. (5*a*) and (11*b*) (neglecting the nonlinear terms), turns the partial differential equations of motion into linear ordinary differential equations in time

$$[M_n]\{\ddot{U}_n(t)\} + [K_n]\{U_n(t)\} = \{F_n(t)\} \tag{26a}$$

where the 7×7 matrices $[M_n]$ and $[K_n]$ are the mass matrix containing the inertial terms and the stiffness matrix of the nth Fourier term, respectively. The rows of the equations of motion in (26*a*) correspond to Eqs. (10*a*), (7), (8), (5*a*), (11*a*), (9), and (6*a*), respectively. The vector of the unknown generalized coordinates are

$$\{U_n(t)\} = \{U_n^b(t), U_n^c(t), \Phi_n^c(t), U_n^t(t), W_n^b(t), W_n^c(t), W_n^t(t)\}^T \tag{26b}$$

and the load vector $\{F_n(t)\} = T(t)\{0,0,0,0,0,0,Q_n\}^T$. The ordinary differential equations can be solved using standard numerical integration methods.

In the next section we will use a particular blast loading case study to assess the accuracy of EHSAPT as well as the earlier HSAPT that does not take into account the axial rigidity of the core. Notice that in this paper we focus on the high-order theories whereas a comparison with the first order shear deformation theory (FOSDT) that does not consider the transverse compressibility of the core was done in Kardomateas et al. [11]. The earlier high-order sandwich panel theory (HSAPT) is outlined in Appendix B.

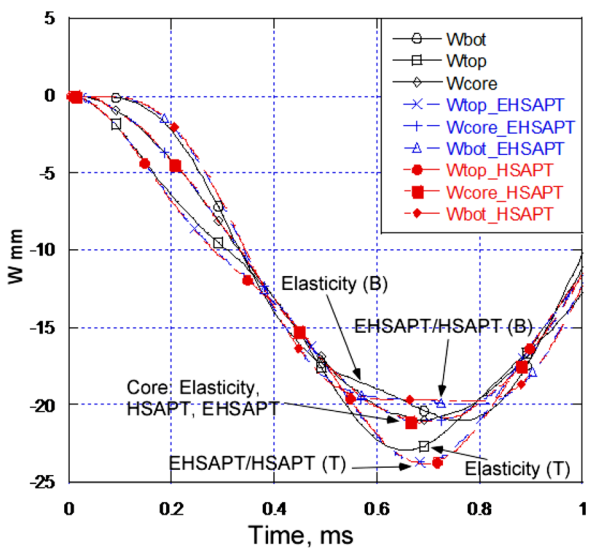

Fig. 2 Transverse displacement at the top face, middle of core, and bottom face at the midspan location for elasticity, EHSAPT, and HSAPT during the initial phase of blast

2.2. Special Case of Exponentially Decaying Blast Loading. In this section the dynamic response of a simply supported sandwich beam, initially at rest, then subjected to a temporal blast load that exponentially decays in time and has a half-sine spatial profile along the beam is studied. Only the first term in the Fourier series is needed. The applied load in kN/m (with time t in milliseconds) is

$$\tilde{q}(x,t) = 510\sin\frac{\pi x}{a}e^{-(1.25t)} \tag{27}$$

which decays to less than 0.1% of its original magnitude after 5.5 milliseconds (ms). The above blast load parameters, as well as the material and geometry data, were taken from the experimental investigations of Gardner et al. [4]. The faces are E-glass vinyl-ester composite: Young's modulus $E_1^c = 13,600$ MPa, density $\rho^f = 1800\,\text{kg/m}^3$, and the isotropic core is Corecell$^{(\text{tm})}$ A300

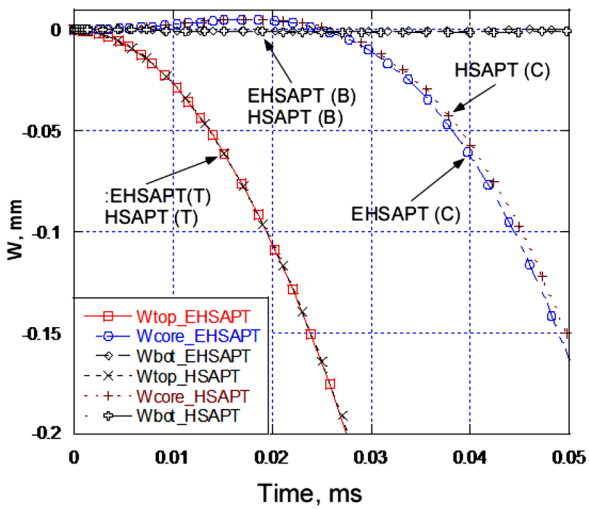

(a)

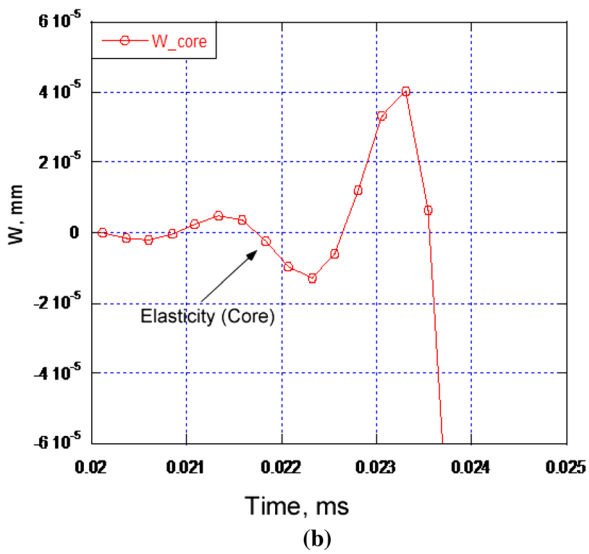

(b)

Fig. 3 (*a*) Transverse displacement at the top face, middle of core, and bottom face at the midspan location from EHSAPT and HSAPT during the first 50 μs showing the cavitation-like behavior of the core. (*b*) Transverse displacement at the middle of core at the midspan location from elasticity showing the cavitation-like behavior of the core around 20 μs.

styrene acrylonitrile (SAN) foam: Young's modulus $E^c = 32$ MPa, $\rho^c = 58.5\,\text{kg/m}^3$, Poisson's ratio $\nu^c = 0.3$, and shear modulus $G^c = E^c/[2(1+\nu^c)]$. The geometry of the sandwich configuration is: face thickness $f_t = f_b = 5$ mm, core thickness $2c = 38$ mm, width $b = 102$ mm, and span of beam $a = 152.4$ mm.

The transverse displacements w_0^t, w_0^c, and w_0^b at the midspan location $x = a/2$ versus time are shown in Fig. 2. In this figure we show the results from elasticity, EHSAPT, and HSAPT. The two high-order sandwich panel theories are practically on top of each other and display the same trend in behavior of the top, core, and bottom displacements as elasticity, i.e., that the top face travels down first, followed by the core, then the bottom face sheet. Differences between the high-order theories and elasticity can be distinguished by focusing on the time between 0.5 and 0.8 ms when the different phases first reach their maximum values as shown in Fig. 2. EHSAPT and HSAPT match the midcore transverse displacement of elasticity. The high order theories overestimate the maximum displacement of the top face by a modest amount, no more than 5%. The bottom face transverse displacements from EHSAPT and HSAPT do not exactly follow elasticity but give values within less than 6% error over the time range in Fig. 2.

It should also be noted that the first order shear deformation theory (FOSDT) can be very inaccurate in its prediction of transverse displacement (Kardomateas et al. [11]) and, of course, cannot capture the differences in the displacements of the face sheets and the core. The FOSDT actually significantly overpredicts the magnitude of the transverse displacement (Kardomateas et al. [11]).

An interesting phenomenon is shown in Fig. 3(*a*). The high-order theories show a very small positive value of the transverse displacement of the core between 15 and 25 μs. Afterwards, the displacement is negative (i.e., in the direction of the blast). This is similar to the cavitation zone in water that occurs behind a shock wave front. The dynamic elasticity also shows such behavior, as shown in Fig. 3(*b*) but at a much smaller scale of positive displacement values.

Figure 4 shows the axial displacements u_0^t, u_0^c, and u_0^b at the edge $x = 0$ versus time. EHSAPT and HSAPT capture the high cyclic behavior of u_0^c that elasticity displays, with EHSAPT being closer in value to elasticity than HSAPT. The first peak in the core axial displacement, u_0^c of EHSAPT, is 10% under elasticity, while the first peak in u_0^c of HSAPT is 32% under elasticity. Both high-order theories and elasticity predict very similar behavior with time of the top and bottom face sheet axial displacements u_0^t and u_0^b.

The transverse stress at the top and bottom face/core interfaces at the midspan σ_{zz} is shown in Fig. 5(*a*). EHSAPT and HSAPT predict similar behavior in stresses versus time. The maximum compressive transverse stress at the top face/core interface predicted by the high order theories (at around 0.23 ms) overpredicts the elasticity value by 5%. The maximum compressive transverse stress at the bottom face/core interface predicted by the high-order theories (at around 0.2 ms) overpredicts the elasticity value by 6%. The high-order theories correctly predict that the bottom face/core interface undergoes a tensile stress at the bottom/face core interface over time. The first maximum tensile transverse stress at the bottom face/core interface predicted by the high-order theories (at around 0.44 ms) overpredicts the elasticity value by 14%.

There is also an associated "cavitation" phenomenon in σ_{zz}, in that a tensile stress wave occurs in the bottom face/core interface just after the blast (within the first 50 μs) as shown in Fig. 5(*b*). Afterwards, the compressive stress wave reaches the bottom face.

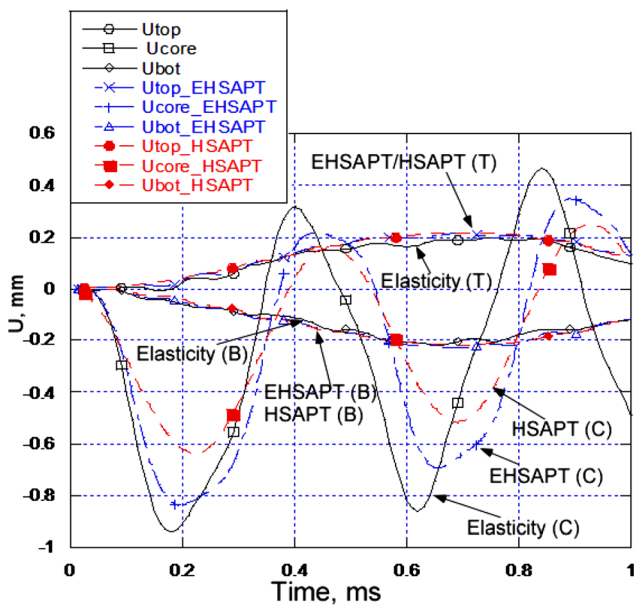

Fig. 4 Axial displacement at the top face, middle of core, and bottom face at the support location ($x = 0$) for elasticity, EHSAPT, and HSAPT during the initial phase of blast

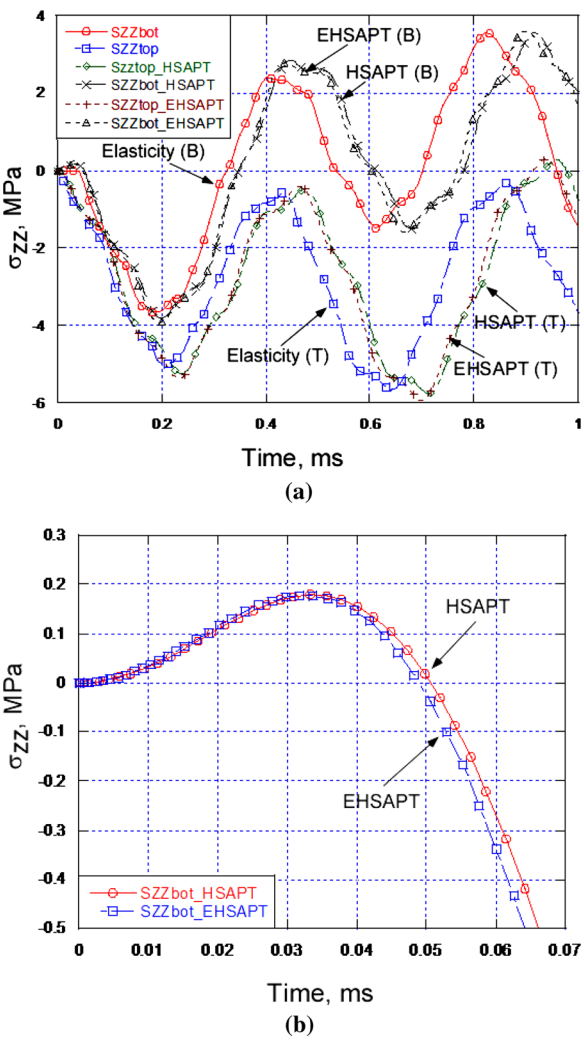

Fig. 5 (*a*) The transverse normal stress σ_{zz}, at the top (T) and bottom (B) face/core interfaces during the initial phase of blast. (*b*) The transverse normal stress σ_{zz} at the bottom face/core interfaces from the high-order theories, showing the cavitation-like behavior (tensile stress during the first 50 μs).

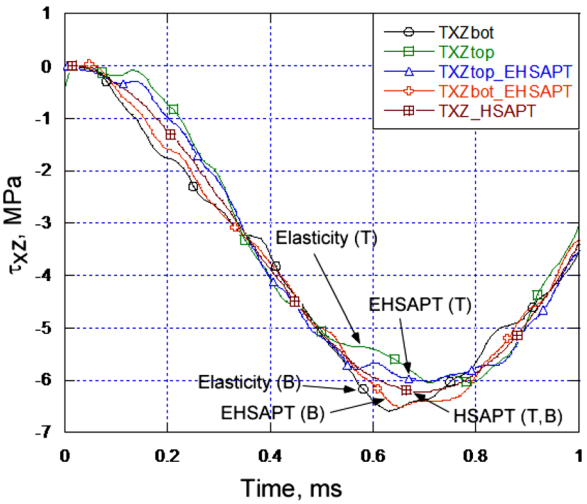

Fig. 6 The shear stress τ_{xz} at the top (T) and bottom (B) face/core interfaces during the initial phase of blast

A similar phenomenon is predicted from the dynamic elasticity within the first 50 μs, albeit at a smaller value of peak tensile stress.

The shear stress at the top and bottom face/core interfaces at $x = 0$ is shown in Fig. 6. EHSAPT is the only theory that can show the differences in the shear stresses at the top and bottom face/core interfaces like elasticity, while HSAPT predicts that the shear stress is constant throughout the thickness and seems to be about the average value of EHSAPT and elasticity. EHSAPT gives a minimum shear stress (most negative shear stress) at the top and bottom face/core interface under the minimum elasticity values by just 0.5%, whereas the corresponding HSAPT values are within 6% of elasticity's predictions.

It was shown in the authors' previous work (Phan et al. [10]) that the HSAPT and EHSAPT show very different behavior in τ_{xz} for soft core and moderate core configurations. The soft core configuration is graphite epoxy faces with a glass phenolic honeycomb core ($E_1^f/E_1^c < 0.001$) and the moderate core configuration is E-glass faces with a Balsa wood core ($E_1^f/E_1^c \sim 0.02$). Details of material data for the two configurations are given in Table 1. Both configurations are for a ratio of face sheet to total thickness $f/h_{\text{tot}} = 0.02$ and a total thickness of $h_{\text{tot}} = 48$ mm, width $b = 25.4$ mm, and length $a = 30\ h_{\text{tot}}$ all other geometric parameters kept the same. It can be seen from Fig. 7(*a*) that for soft cores the shear stresses at the top and bottom face/core interfaces can be very different, as predicted by the EHSAPT. For the soft core case the HSAPT predicts an average value of the shear stress at the top and bottom face core interfaces. The picture is very different for the moderate core case (Fig. 7(*b*)), which shows that the HSAPT predicts a shear stress that is not between the top and bottom interface shear stresses but overpredicts the magnitude of the negative shear stress of the top and bottom face/core interfaces by about 10%.

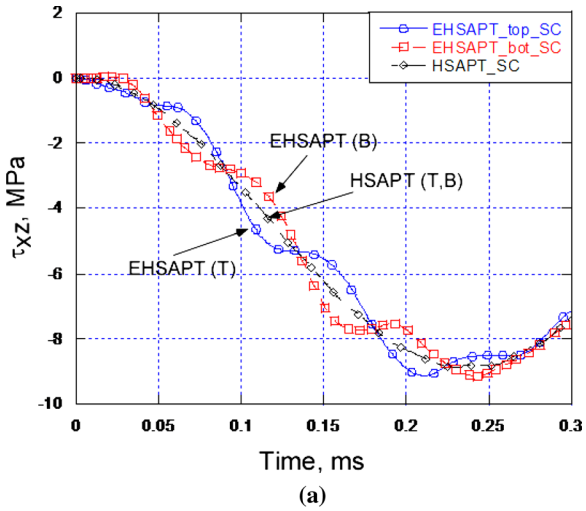

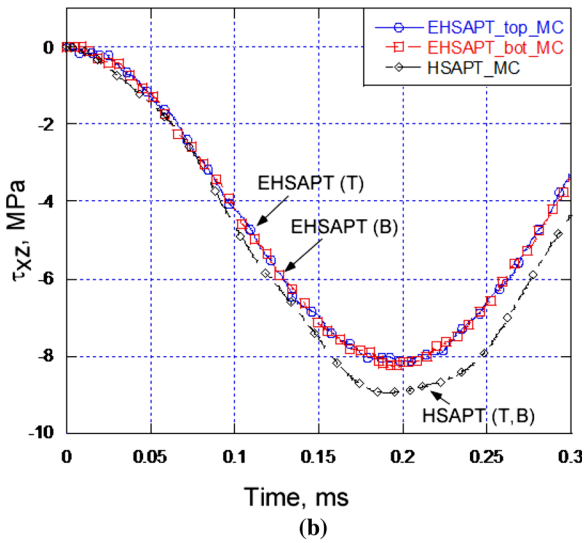

Fig. 7 (*a*) The shear stress τ_{xz} at the top (T) and bottom (B) face/core interfaces from the higher-order theories for the soft core configuration. (b) The shear stress τ_{xz} at the top (T) and bottom (B) face/core interfaces from the higher order theories for the moderate core configuration.

Table 1 Material properties. Moduli data are in GPa. Densities are in kg/m^3

	Graphite epoxy face	E-glass polyester face	Balsa wood core	Glass-phenolic honeycomb core
E_1	181.0	40.0	0.671	0.032
E_2	10.3	10.0	0.158	0.032
E_3	10.3	10.0	7.72	0.300
G_{23}	5.96	3.5	0.312	0.048
G_{31}	7.17	4.5	0.312	0.048
G_{12}	7.17	4.5	0.200	0.013
ν_{32}	0.40	0.40	0.49	0.25
ν_{31}	0.016	0.26	0.23	0.25
ν_{12}	0.277	0.065	0.66	0.25
ρ	1632	2000	250	64

Conclusions

The dynamic formulation of the extended high-order sandwich panel theory (EHSAPT) is accomplished via the Hamilton's principle for a general asymmetric sandwich configuration, and nonlinear axial strains of the face sheets are taken into account. The solution procedure to determine the linear dynamic response of a sandwich composite that is simply supported and loaded just on the top face sheet is outlined. A case study involving an exponentially decaying blast load with a spatial half-sine profile across the top of the beam is used to compare the EHSAPT and the earlier high-order sandwich panel theory (HSAPT) to a dynamic elasticity benchmark. The case study showed that both theories capture well the general trends of the transverse and axial displacements, as well as the transverse normal and shear stresses, with the EHSAPT being more accurate, i.e., closer to the dynamic elasticity. The high-order theories predict well the complex nature of the transient response to blast, including a "cavitation-like" phenomenon during the first 50 μs, i.e., a tensile transverse stress wave and displacement opposite to the direction of the blast at the bottom face/core interface.

Acknowledgment

The financial support of the Office of Naval Research, Grant N00014-11-1-0597 and the interest and encouragement of the grant monitor, Dr. Y. D. S. Rajapakse, are both gratefully acknowledged.

Appendix A Mass and Stiffness Matrix for the EHSAPT

The mass matrix $[M_n]$ is symmetric and contains elements $m_{ij} = m_{ji}$. With the definition $\alpha_n = n\pi/a$, these are (per unit width):

$$m_{11} = f_b\rho^b + \frac{6c\rho^c}{35}; \quad m_{12} = \frac{2c\rho^c}{15} \tag{A1a}$$

$$m_{13} = -\frac{2c^2\rho^c}{35}; \quad m_{14} = \frac{c\rho^c}{35} \tag{A1b}$$

$$m_{15} = -\frac{3cf_b\rho^c\alpha_n}{35}; \quad m_{16} = 0; \quad m_{17} = \frac{cf_t\rho^c\alpha_n}{70} \tag{A1c}$$

$$m_{22} = \frac{16c\rho^c}{15}; \quad m_{23} = 0; \quad m_{24} = m_{12} \tag{A1d}$$

$$m_{25} = -\frac{cf_b\rho^c\alpha_n}{15}; \quad m_{26} = 0; \quad m_{27} = \frac{cf_t\rho^c\alpha_n}{15} \tag{A1e}$$

$$m_{33} = \frac{16c^3\rho^c}{105}; \quad m_{34} = \frac{2c^2\rho^c}{35} \tag{A1f}$$

$$m_{35} = \frac{c^2f_b\rho^c\alpha_n}{35}; \quad m_{36} = 0; \quad m_{37} = \frac{c^2f_t\rho^c\alpha_n}{35} \tag{A1g}$$

$$m_{44} = \frac{6c\rho^c}{35} + f_t\rho^t; \quad m_{45} = -\frac{cf_b\rho^c\alpha_n}{70} \tag{A1h}$$

$$m_{46} = 0; \quad m_{47} = \frac{3cf_t\rho^c\alpha_n}{35} \tag{A1i}$$

$$m_{55} = f_b\rho_b + \frac{4c\rho^c}{15} + \left(\frac{f_b^3\rho_b}{12} + \frac{3cf_b^2\rho^c}{70}\right)\alpha_n^2; \quad m_{56} = m_{12} \tag{A1j}$$

$$m_{57} = -\frac{c\rho^c}{15} - \frac{cf_bf_t\rho^c\alpha_n^2}{140} \tag{A1k}$$

$$m_{66} = \frac{16c\rho^c}{15}; \quad m_{67} = m_{12} \tag{A1l}$$

$$m_{77} = \frac{4c\rho_c}{15} + f_t\rho^t + \left(\frac{3cf_t^2\rho^c}{70} + \frac{f_t^3\rho^t}{12}\right)\alpha_n^2 \tag{A1m}$$

The stiffness matrix $[K_n]$ is also symmetric and contains elements $k_{ij} = k_{ji}$, which are as follows (per unit width):

$$k_{11} = \frac{47}{30c}C_{55}^c + \alpha_1^b\alpha_n^2; \quad k_{12} = -\frac{4}{3c}C_{55}^c + \frac{2c\alpha_n^2}{15}C_{11}^c \tag{A2a}$$

$$k_{13} = \frac{4}{5}C_{55}^c - \frac{2c^2\alpha_n^2}{35}C_{11}^c; \quad k_{14} = -\frac{7}{30c}C_{55}^c + \frac{c\alpha_n^2}{35}C_{11}^c \tag{A2b}$$

$$k_{15} = -\left(\frac{3cf_b\alpha_n^3}{35}C_{11}^c + \eta_3^b\alpha_n\right); \quad k_{16} = -\beta_1\alpha_n;$$
$$k_{17} = \frac{cf_t\alpha_n^3}{70}C_{11}^c + \eta_2^t\alpha_n \tag{A2c}$$

$$k_{22} = \frac{8}{3c}C_{55}^c + \frac{16c\alpha_n^2}{15}C_{11}^c; \quad k_{23} = 0; \quad k_{24} = k_{12} \tag{A2d}$$

$$k_{25} = -\frac{cf_b\alpha_n^3}{15}C_{11}^c + \eta_6^b\alpha_n; \quad k_{26} = 0; \quad k_{27} = \frac{cf_t\alpha_n^3}{15}C_{11}^c - \eta_6^t\alpha_n \tag{A2e}$$

$$k_{33} = \frac{8c}{5}C_{55}^c + \frac{16c^3\alpha_n^2}{105}C_{11}^c; \quad k_{34} = -\frac{4}{5}C_{55}^c + \frac{2c^2\alpha_n^2}{35}C_{11}^c \tag{A2f}$$

$$k_{35} = \frac{c^2f_b\alpha_n^3}{35}C_{11}^c - \eta_4^b\alpha_n; \quad k_{36} = \frac{4c\beta_1\alpha_n}{3};$$
$$k_{37} = \frac{c^2f_t\alpha_n^3}{35}C_{11}^c - \eta_4^t\alpha_n \tag{A2g}$$

$$k_{44} = \frac{47}{30c}C_{55}^c + \alpha_1^t\alpha_n^2; \quad k_{45} = -\left(\frac{cf_b\alpha_n^3}{70}C_{11}^c + \eta_2^b\alpha_n\right) \tag{A2h}$$

$$k_{46} = \beta_1\alpha_n; \quad k_{47} = \frac{3cf_t\alpha_n^3}{35}C_{11}^c + \eta_3^t\alpha_n \tag{A2i}$$

$$k_{55} = \frac{7}{6c}C_{33}^c - \eta_8^b\alpha_n^2 + \eta_9^b\alpha_n^4; \quad k_{56} = -\left(\frac{4}{3c}C_{33}^c + \eta_7^b\alpha_n^2\right) \tag{A2j}$$

$$k_{57} = \frac{1}{6c}C_{33}^c - \frac{cf_bf_t\alpha_n^4}{140}C_{11}^c - \beta_2\alpha_n^2 \tag{A2k}$$

$$k_{66} = \frac{8}{3c}C_{33}^c + \frac{16c\alpha_n^2}{15}C_{55}^c; \quad k_{67} = -\left(\frac{4}{3c}C_{33}^c + \eta_7^t\alpha_n^2\right) \tag{A2l}$$

$$k_{77} = \frac{7}{6c}C_{33}^c - \eta_8^t\alpha_n^2 + \eta_9^t\alpha_n^4 \tag{A2m}$$

Appendix B High-Order Sandwich Panel Theory (HSAPT)

The high-order sandwich panel theory accounts for the shear and transverse normal stresses in the core and assumes that the axial stresses in the core are null. There are two models of HSAPT that exist in literature. The first model (model I) is a mixed formulation in which the five generalized coordinates are: the two axial displacements at the top and bottom face sheet $u_0^t(x)$, $u_0^b(x)$; the two transverse displacements at the top and bottom face sheets $w_0^t(x)$, $w_0^b(x)$; and the shear stress (constant through the thickness) in the core and $\tau^c(x)$. In model I, the accelerations are assumed a

priori to vary linearly through the core. The second model (model II) is a displacement based formulation in which the five generalized coordinates are: $u_0^t(x)$, $u_0^b(x)$, $w_0^t(x)$, $w_0^b(x)$, and the midcore transverse displacement $w_0^c(x)$ (instead of the shear stress $\tau^c(x)$). In model II, the accelerations in the core are allowed to be nonlinear through the core.

HSAPT–mixed formulation (model I). The free vibration analysis for the mixed formulation (model I) was presented in detail in Schwarts-Givli et al. [12]. The mass and stiffness matrix are explicitly written for the free vibration of a sandwich beam that is simply supported throughout its thickness at each end. In the mixed formulation $u^c(x,z,t)$ and $w^c(x,z,t)$ are functions of $\tau^c(x,t)$.

HSAPT–displacements based formulation (model II). In this formulation, the generalized coordinate of shear stress $\tau^c(x,t)$ is replaced with the midcore transverse displacement $w_0^c(x,t)$. The axial and transverse displacement fields of the top and bottom face sheet, as well as the transverse displacement field of the core are the same as ESHAPT shown in Eqs. (1) and (2*a*). Model II differs from EHSAPT in that the axial displacement field between $-c < z < c$ is defined as

$$u^c(x,z,t) = \left(\frac{1}{2}+\frac{z}{2c}\right)u_0^t(x,t) + \left(\frac{1}{2}-\frac{z}{2c}\right)u_0^b(x,t) + \left(-\frac{z}{3}+\frac{z^3}{3c^2}\right)w_{0,x}^c(x,t) + \left[-\left(\frac{f_b}{4}+\frac{c}{4}\right) + \left(\frac{1}{6}+\frac{f_b}{4c}\right)z + \frac{1}{4c}z^2 - \frac{1}{6c^2}z^3\right]w_{0,x}^b(x,t) + \left[\left(\frac{f_t}{4}+\frac{c}{4}\right) + \left(\frac{1}{6}+\frac{f_t}{4c}\right)z - \frac{1}{4c}z^2 - \frac{1}{6c^2}z^3\right]w_{0,x}^t(x,t) \tag{B1}$$

The governing equations of motion of a simply supported sandwich beam undergoing the load in Eq. (23) using HSAPT is in general the 5×5 system of equations:

$$[M_n]\{\ddot{U}_n(t)\} + [K_n]\{U_n(t)\} = \{F_n(t)\} \tag{B2}$$

where the 5×5 matrices $[M_n]$ and $[K_n]$ are the mass matrix containing the inertial terms and the stiffness matrix of the nth Fourier term, respectively.

The 5×5 symmetric mass matrix for the HSAPT, having $m_{ij} = m_{ji}$, is (per unit width)

$$m_{11} = \frac{1}{3}\left(3f_b\rho^b + 2c\rho^c\right); \quad m_{12} = \frac{1}{3}c\rho^c \tag{B3a}$$

$$m_{13} = -\frac{1}{90}c\rho^c\alpha_n(30f_b+17c); \quad m_{14} = \frac{2}{45}c^2\rho^c\alpha_n \tag{B3b}$$

$$m_{15} = \frac{1}{90}c\rho^c\alpha_n(13c+15f_t) \tag{B3c}$$

$$m_{22} = \frac{1}{3}(2c\rho^c + 3f_t\rho^t); \quad m_{23} = -\frac{1}{90}c\rho^c\alpha_n(15f_b+13c) \tag{B3d}$$

$$m_{24} = -\frac{2}{45}c^2\rho^c\alpha_n; \quad m_{25} = \frac{1}{90}c\rho^c\alpha_n(17c+30f_t) \tag{B3e}$$

$$m_{33} = \frac{1}{72}\left[\frac{2\alpha_n^2}{105}(714c^2f_b\rho^c + 630cf_b^2\rho^c + 315f_b^3\rho^b + 268c^3\rho^c) + \frac{24}{5}(15f_b\rho^b + 4c\rho^c)\right] \tag{B3f}$$

$$m_{34} = \frac{1}{72}\left[\frac{2}{105}\left(-84c^2f_b\rho^c\alpha_n^2 - 32c^3\rho^c\alpha_n^2\right) + \frac{48c\rho^c}{5}\right] \tag{B3g}$$

$$m_{35} = \frac{1}{72}\left[-\frac{2}{105}c\rho^c\alpha_n^2\left(273c(f_b+f_t) + 315f_bf_t + 236c^2\right) - \frac{24c\rho^c}{5}\right] \tag{B3h}$$

$$m_{44} = \frac{1}{36}\left(\frac{64}{105}c^3\rho^c\alpha_n^2 + \frac{192c\rho^c}{5}\right) \tag{B3i}$$

$$m_{45} = \frac{1}{36}\left[\frac{24c\rho^c}{5} - \frac{4}{105}c^2\rho^c\alpha_n^2(8c+21f_t)\right] \tag{B3j}$$

$$m_{55} = \frac{\alpha_n^2[2c\rho^c(134c^2+357cf_t+315f_t^2)+315f_t^3\rho^t]}{3780} + \frac{1}{15}(4c\rho^c + 15f_t\rho^t) \tag{B3k}$$

and the 5×5 symmetric stiffness matrix with $k_{ij} = k_{ji}$ has the following elements (per unit width):

$$k_{11} = \frac{G_{31}^c}{2c} + f_bE_1^b\alpha_n^2 \tag{B4a}$$

$$k_{12} = -\frac{G_{31}^c}{2c}; \quad k_{13} = -\frac{G_{31}^c\alpha_n(3f_b+2c)}{12c} \tag{B4b}$$

$$k_{14} = -\frac{2}{3}G_{31}^c\alpha_n; \quad k_{15} = -\frac{G_{31}^c\alpha_n(2c+3f_t)}{12c} \tag{B4c}$$

$$k_{22} = \frac{G_{31}^c}{2c} + f_t\alpha_n^2E_1^t \tag{B4d}$$

$$k_{23} = \frac{G_{31}^c\alpha_n(3f_b+2c)}{12c}; \quad k_{24} = \frac{2}{3}G_{31}^c\alpha_n \tag{B4e}$$

$$k_{25} = \frac{G_{31}^c\alpha_n(2c+3f_t)}{12c} \tag{B4f}$$

$$k_{33} = \frac{1}{72}\left[\frac{G_{31}^c\alpha_n^2(3f_b+2c)^2}{c} + 6f_b^3E_1^b\alpha_n^4 + \frac{84E_3^c}{c}\right] \tag{B4g}$$

$$k_{34} = \frac{1}{72}\left[8G_{31}^c\alpha_n^2(3f_b+2c) - \frac{96E_3^c}{c}\right] \tag{B4h}$$

$$k_{35} = \frac{1}{72}\left[\frac{G_{31}^c\alpha_n^2(3f_b+2c)(2c+3f_t)}{c} + \frac{12E_3^c}{c}\right] \tag{B4i}$$

$$k_{44} = \frac{1}{36}\left(32cG_{31}^c\alpha_n^2 + \frac{96E_3^c}{c}\right);$$
$$k_{45} = \frac{1}{36}\left[4G_{31}^c\alpha_n^2(2c+3f_t) - \frac{48E_3^c}{c}\right] \tag{B4j}$$

$$k_{55} = \frac{G_{31}^c\alpha_n^2(2c+3f_t)^2}{72c} + \frac{7E_3^c}{6c} + \frac{1}{12}f_t^3\alpha_n^4E_1^t \tag{B4k}$$

The vector of the unknown generalized coordinates in Eq. (B2) is

$$\{U_n(t)\} = \{U_n^b(t), U_n^t(t), W_n^b(t), W_n^c(t), W_n^t(t)\}^T \tag{B5}$$

and the load vector $\{F_n(t)\} = T(t)\{0,0,0,0,Q_n\}^T$. The ordinary differential Eq. (B2) in time can be solved using standard numerical integration methods.

References

[1] Allen, H.G., 1969, *Analysis and Design of Structural Sandwich Panels*, Pergamon Press, Oxford, UK.

[2] Plantema, F.J., 1966, *Sandwich Construction*, Wiley, New York.

[3] Kardomateas, G.A., and Phan, C. N., 2011, "Three-Dimensional Elasticity Solution for Sandwich Beams/Wide Plates With Orthotropic Phases: the Negative Discriminant Case," J. Sandwich Struct. Mat., **13**(6), pp. 641–661.

[4] Gardner, N., Wang, E., Kumar, P., and Shukla, A., 2011, "Blast Mitigation in a Sandwich Composite Using Graded Core and Polyurea Interlayer," Exper. Mech., **52**(2), pp. 119–133.
[5] Jackson, M., and Shukla, A., 2011, "Performance of Sandwich Composites Subjected to Sequential Impact and Air Blast Loading," Composit. B Eng., **42**(2), pp. 155–166.
[6] Wang, E., and Shukla, A., 2011, "Blast Performance of Sandwich Composites With In-Plane Compressive Loading," Exper. Mech., **52**(1), pp. 49–58.
[7] Tekalur, S. A., Bogdanovich A. E., and Shukla, A., 2009, "Shock Loading Response of Sandwich Panels With 3-D Woven E-Glass Composite Skins and Stitched Foam Core," Compos. Sci. Tech., **69**(6), pp. 736–753.
[8] Wang, E., Gardner, N., and Shukla, A., 2009, "The Blast Resistance of Sandwich Composites With Stepwise Graded Cores," Int. J. Solid. Struct., **46**(18), pp. 3492–3502.
[9] Frostig, Y., Baruch, M., Vilnay O., and Sheinman I., 1992, "High-Order Theory for Sandwich-Beam Behavior With Transversely Flexible Core," J. Eng. Mech., **118**(5), pp. 1026–1043.
[10] Phan, C. N., Frostig, Y., and Kardomateas, G. A., 2012, "Analysis of Sandwich Panels With a Compliant Core and With In-Plane Rigidity-Extended High-Order Sandwich Panel Theory Versus Elasticity," ASME J. Appl. Mech., **79**, p. 041001.
[11] Kardomateas, G. A., Frostig, Y., and Phan, C. N., 2012, "Dynamic Elasticity Solution for the Transient Blast Response of Sandwich Beams/Wide Plates, AIAA J., **51**(2), pp. 485–491.
[12] Schwarts-Givli, H., Rabinovitch, O., and Frostig, Y., 2008, "Free Vibration of Delaminated Unidirectional Sandwich Panels With a Transversely Flexible Core and General Boundary Conditions—A High Order Approach," J. Sandwich Struct. Mat., **10**(2), pp. 99–131.